Citation for published version:
Qiang, T, Song, Y & James, TD 2020, 'Hierarchically porous zirconium dioxide dual-templated by acacia mangium tannin extract and an amphiphilic triblock copolymer', *Materials Chemistry and Physics*, vol. 253, 123335. https://doi.org/10.1016/j.matchemphys.2020.123335

DOI:
10.1016/j.matchemphys.2020.123335

Publication date:
2020

Document Version
Peer reviewed version

Link to publication

Publisher Rights
CC BY-NC-ND

University of Bath

Alternative formats
If you require this document in an alternative format, please contact:
openaccess@bath.ac.uk

General rights
Copyright and moral rights for the publications made accessible in the public portal are retained by the authors and/or other copyright owners and it is a condition of accessing publications that users recognise and abide by the legal requirements associated with these rights.

Take down policy
If you believe that this document breaches copyright please contact us providing details, and we will remove access to the work immediately and investigate your claim.

Download date: 05. May. 2023

Hierarchically porous zirconium dioxide dual-templated by *acacia mangium tannin extract* and an amphiphilic triblock copolymer

Taotao Qiang [*, †], Yunying Song [†], Tony D. James[**, ‡]

[†]College of Bioresources Chemical and Materials Engineering, Shaanxi University of Science & Technology, Xi'an 710021, Shaanxi, China; National Demonstration Center for Experimental Light Chemistry Engineering Education (Shaanxi University of Science & Technology), Xi'an 710021, China.

[‡] Department of Chemistry, University of Bath, Bath BA2 7AY, United Kingdom

*Corresponding author. College of Bioresources and Materials Engineering, Shaanxi University of Science & Technology, Xi'an, Shaanxi 710021, PR China

E-mail address: qiangtt515@163.com. Tel: 029-86132530

[**] Corresponding author. Department of Chemistry, University of Bath, Bath BA2 7AY, United Kingdom

Email: t.d.james@bath.ac.uk

Abstract: In this article, a new hierarchical porous zirconia material with adjustable pore size is fabricated by using biomass materials of *acacia mangium tannin extract* (AMTE) and amphiphilic triblock copolymer poly(ethylene glycol)-blockpoly(propylene glycol)-block-poly(ethylene glycol) (P123) as a dual-template for the first time. All the raw materials we used are non-toxic and the synthesis process is relatively simple, low-cost, eco-friendly, and reproducible, which is suitable for large-scale production. Characterization using SEM, N_2 sorption isotherm, and Mercury intrusion porosimetry indicate that hierarchical porous ZrO_2 combining abundant mesopores and macropores was synthesized successfully using P123 and AMTE as a dual template. Significantly, dual-templated ZrO_2 with hierarchical porosity has an advantage over single-templated samples in protein adsorption, especially for the large-sized proteins. Furthermore, the real sample test shows the synthesized material with a multidimensional porous structure displays the potential for practical protein wastewater treatment.

KEYWORDS: biomass material, dual template method, hierarchical porous ZrO_2, adsorption of proteins, real sample application.

1. Introduction

Protein substances can be discharged into wastewater during food production and leather making, resulting in not only the eutrophication of water but is also a waste of resource. Therefore, it is crucial to find suitable materials for adsorption and separation of proteins from wastewater, which will provide the possibility for further protein purification and utilization in the field of pharmaceutical industry, food processing, and biotechnology sectors [1, 2]. Accordingly, significant efforts have been devoted to develop adsorbents possessing high adsorption capacity and good separation efficiency.

Generally, the materials with larger pore diameter like mesoporous (2~50 nm) [3] or macroporous (>50 nm) [4] are beneficial for the adsorption of bio macromolecules such as proteins, nucleic acids and enzymes. However, the pore diameter of mesoporous materials is mostly around 5 nm, limiting the practical application including the transport of large sized biomolecules [5]. While, the synthesis of mesoporous materials with larger pore diameter have disadvantages such as complicated synthetic procedures or expensive template agents, which make them unsuitable for commercial applications [6, 7]. Moreover, the macroporous material easily collapse during calcination under higher temperature due to the particle's growth [8, 9]. Therefore, hierarchical porous materials have attracted a lot of attention from researchers ever since the first macroporous-mesoporous materials were reported in 1998 by Yang *et al*, which offered technological promise for many applications [10]. In order to adsorb and separate bio macromolecules, porous materials with mesoporous and macroporous structure are desired because the interconnected macropores can promote fast mass-transfer, while the mesotexture can enlarge the surface area. In addition, hierarchical porous materials can provide better accessibility for adsorbates to the active sites compared with other materials with single-sized porous structures [11, 12]. Zirconium oxide, a non-toxic conventional metallic oxide, has gained much attention owing to its attractive properties like acid-base activity, chemical stability, thermal stability, and biocompatibility [13-16]. Therefore, preparation of zirconium oxide with multidimensional porosity,

combining the advantages of mesopores and macropores, provides promising matrices to separate bio macromolecular species.

Several approaches like the template method are currently available for the synthesis of porous structural materials [17, 18]. Surfactant templating agents, such as ionic surfactants, nonionic surfactants and fluorocarbon surfactants, are commonly used to synthesize ordered micro- and mesoporous materials [19]. For example, Chen *et al.* [20] have synthesized a zirconia film with single mesoporous structure of 3.5 nm by using Tween 20 as a template and acetylacetone as a chelating agent, resulting in a material with good structural integrity and electrochemical properties. While, With and co-workers [21] have developed a two-step synthetic method to prepare zirconium oxide with defined hierarchical porous structure, among which spherical activated carbon acted as an exotemplate and triblock copolymer acted as an endotemplate. The synthesized nanoparticle resulted in hierarchical mesopores with maxima at ca. 3 and 20 nm.

Normally, the pore size of porous materials based on a single-template of surfactant micelles is small, which limits their encapsulation ability for biological macromolecules [22]. Moreover, complicated synthetic procedure is the major drawback for the synthesis of hierarchical porous materials using a dual-templating method. Therefore, we report our research towards a simple and environmentally friendly approach to prepare porous nanoparticles with desirable and distinctive hierarchical porosity.

Acacia mangium tannin extract (AMTE), extracted from vegetables, is a polymer of catechin units with multiple phenolic groups [23]. It is a templating agent because it possesses an amphiphilic nature by virtue of phenolic hydroxyl and sulfonic groups as hydrophilic sites and aromatic rings as hydrophobic sites, which can form micelles in aqueous solution. Another advantage of using AMTE biomass material as a template is its environmental-friendly and sustainable properties in addition to low-cost. Our aim is to take advantage of biomass materials like AMTE as templating agents to prepare hierarchical porous materials, which can be applied for the adsorption and separation of biological molecules.

In this study, hierarchical porous zirconia with adjustable porosity was synthesized by combining traditional triblock block copolymer Pluronic P123, vegetable tanning agent AMTE as dual-templating, and inorganic metal salt zirconium sulfate as metal source (Scheme 1). It should be noted that AMTE is not only a templating agent but also a polydentate ligand, which can assist in controlling the hydrolysis rate of inorganic metal salt due to its capability of forming complexes with metal ions. Meanwhile, P123 acts as a template for the mesopores and a stabilizing agent for the zirconia framework [24]. Compared with conventional single porosity materials, hierarchical porous architectures have the superiority in adsorption of larger hydrodynamic sized proteins, which provides the potential for the adsorption and regeneration of proteins from wastewater.

Scheme 1. Schematic illustration of one-pot process used to synthesize hierarchical porous ZrO_2 materials.

2. Experimental section

2.1 Experimental materials

Triblock copolymer poly (ethylene glycol)-blockpoly (propylene glycol)-block-poly (ethylene glycol) (P123) was obtained from Aldrich. The metal source of zirconium sulfate ($Zr(SO_4)_2$•$4H_2O$) was supplied by Tianjin Guanfu Fine Chemical Research Institute Co., Ltd. Biomass template of *acacia mangium tannin extract* (AMTE) was obtained from Sichuan Decision Chemical Co., Ltd., China. The biological protein of Lysozyme (Lyz) and Bovine serum albumin (BSA) were supplied by Maya Reagent., Ltd and Shanghai Lanji biological Co., Ltd. Sodium dihydrogen phosphate (NaH_2PO_4) and disodium hydrogen phosphate (Na_2HPO_4) were purchased from Tianjin Tianli Chemical Reagent Co., Ltd and Tianjin Kemiou Chemical Reagent Co., Ltd,

respectively. Absolute ethyl alcohol was provided by Tianjin Fuyu fine chemical industry Co., Ltd. Softening wastewater was obtained from Hebei Dongming Cowhide Leather Co., Ltd.

2.2 Synthesis of hierarchical porous zirconia

Hierarchical porous zirconia was synthesized by combining P123 and AMTE as dual templates and non-toxic $Zr(SO_4)_2$ as zirconium source without additional additives. Typically, different amounts of P123 and AMTE was dissolved into ethyl alcohol (20 mL) and deionized water (30 mL) respectively, followed by stirring for 20 min under air. Then, different amounts of $Zr(SO_4)_2$ was added into the above system and stirred for another 3 hours. The solution was then aged for 48 h under 40 ℃ in the oven and followed by drying at 60 ℃ for another 24 h. Finally, hierarchical porous zirconia was obtained successfully by calcination (250 ℃, 100 min, 1 ℃/min→600 ℃, 4 h, 2 ℃/min).

2.3 Characterization

The thermogravimetric (TG) curve was obtained using a Bruker thermogravimetric analyzer from 30 to 800 °C with an increment speed of 10°C min^{-1} under a nitrogen atmosphere. X-ray photoelectron spectra were employed to evaluate the elemental composition. The measurement was carried out on X-ray photoelectron spectroscopy instrument (XPS, Axis Ultra) with a monochromatic X-rays source (Al Kα, hν = 1486 eV). X-ray diffraction (XRD, Bruker D8 Advance) patterns were carried out using a powder diffractometer with Cu-Kα radiation (45 kV, 45 mA) in the 2θ range of 1~80 °. The N_2 sorption isotherms were used to evaluate the specific surface areas and relative pore parameters by a Micromeretics ASAP 2460. And prior to the experimental operation, the ZrO_2 samples need to degas for 4 h under vacuum (10-3 Torr, 150 ℃). Mercury intrusion porosimetry was used to evaluate the size distribution of macroporosity at a pressure range of 2.50~33000.00 Psia, and the measurement was carried out on the mercury porosimeter of Auto pore 9500. Scanning electron microscopy (SEM) was employed to observe the microstructure of the samples, which was operated on a FEI Verios 460 microscope at voltages between 5 and 15 kV. The further analysis of the micropore structure was performed by transmission electron

microscope (TEM) by FET Tecnai G2 F20 S-TWIN electron microscope. Fourier transform infrared spectrophotometer (PerkinElmer Spectrum 100) was employed to collect Fourier transform infrared (FT-IR) spectrogram of the samples by KBr tableting method in the wavelength range of 4000-200 cm^{-1}.

2.4 Adsorption experiment

In order to evaluate the adsorption capacity of hierarchical porous ZrO_2 for protein with large molecular size, two kinds of proteins of Bovine serum albumin (BSA, 66000 Da) and Lysozyme (Lyz, 13750 Da) were chosen. Firstly, BSA and Lyz solutions were prepared in PBS buffer solution (pH 4.5, 5, 6, 7, 8, 9) to investigate the optimal pH adsorption conditions. 0.1 g of ZrO_2 was used to adsorb 10 mL protein solution (0.5 mg/mL) at room temperature for 6 hours. Afterward, the mixture was centrifuged and the supernatant was measured by spectrophotometry at the wavelength of 280 nm. The adsorption capacity (q) was calculated as below:

$$q = \frac{(C_0 - C)V}{M} \quad (1)$$

where C_0, C (g/L) are the initial and equilibrium concentration of protein solution, respectively; V (L), M (g) represent the volume of solution and the mass of adsorbent.

In order to analyze the adsorption behavior of ZrO_2 towards proteins, 0.8 g ZrO_2 was used to adsorb 80 mL Lyz solution at pH 4.5. After different adsorption time points (60, 120, 180, 240, 300, 360, 480, 600, 720 min), a sample was taken to measure the absorbance. The kinetic models of pseudo-first-order (PFO) and pseudo-second-order (PSO) were used to fit the experimental data using the following equations [25]:

$$ln(q_e - q_t) = lnq_e - k_1 t \quad (2)$$

$$t/q_t = 1/k_2 {q_e}^2 + t/q_e \quad (3)$$

where q_e represents the adsorption capacities (mg/g) of ZrO_2 samples at equilibrium time t (min). k_1 (min^{-1}) and k_2 (g/mg/ min) are the equilibrium rate constants of kinetic models, respectively.

Adsorption isotherm was another index to evaluate the adsorption mechanism of ZrO_2 samples on proteins. Different concentration (0.2, 0.3, 0.4, 0.5, 0.6, 0.7, 0.8, 0.9 mg/mL) of Lyz solutions were used to measure the adsorption capacity of ZrO_2. The

Langmuir and Freundlich models were carried out to fit experimental data as follows [26]:

$$q_e = bQ_mC_e/(1 + bC_e) \quad (4)$$

$$lnq_e = ln\,k + {}^{1}/_{n}\,lnC_e \quad (5)$$

where Q_m (mg/g) represents the saturated adsorption capacity of ZrO_2 samples; b (L/g) represents the Langmuir constant; k and n are Freundlich constants.

In order to evaluate the adsorption advantage of hierarchical porous ZrO_2 on proteins with larger molecular size, the proteins Lyz and BSA were adsorbed by different ZrO_2 materials for 6 h at room temperature. Afterward, the protein solution was centrifuged (5000 r/min) and the supernatant was measured by spectrophotometry.

2.5 Real-sample test

Finally, leather softening wastewater was used as a real-sample to evaluate the practical protein adsorption capacity of the hierarchical porous ZrO_2. The adsorption process was the same as 2.4. Afterward, the suspension was separated by centrifugation for 5 min at a rate of 5000 r/min and the method Coomassie Brilliant Blue G-250 [27] was used to measure the protein content of wastewater before and after adsorption. The final supernatant was monitored using a UV-vis spectrophotometer at wavelengths between 500~800 nm.

3. Results and discussion

3.1 Characterization

3.1.1 Pyrolysis temperature

Prior to the calcination of the zirconia/templates composites, pyrolysis temperature was evaluated to determine the calcination temperature. TG curve of the zirconia/templates composite in Fig. 1 shows three stages of degradation in the range of 0~800 °C. The first stage (100~200 ℃) corresponds to the volatilization of adsorbed water and residual ethanol solvent in the sample. The second stage (450~500 ℃) is due to the pyrolysis of the organic template materials (P123 and AMTE) in the samples. The mass loss in the third stage (550~600 ℃) is attributed to the removal of SO_4^{2-} ions present in the Zr-O framework [28]. There is nearly no weight loss at temperatures

higher than 600 ℃, indicating the decomposition tended to completion. Therefore, hierarchical porous zirconia was obtained for this research by calcination above 600 ℃.

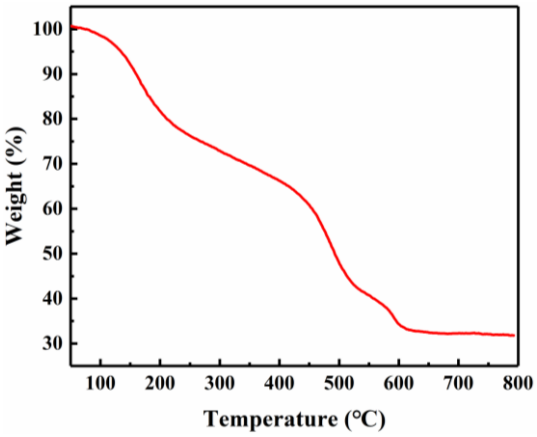

Fig. 1. TG curve of zirconia/templates composite.

3.1.2 Chemical composition and crystal structure

After the preparation of the material, full-survey XPS (Fig.S1a) demonstrates the sample contains Zr and O elements with the peaks located at 181.2 eV (Zr 3d) and 528.6 eV (O 1S) respectively [29]. And two major peaks around 182.1 eV and 184.4 eV in Fig. S1b corresponds to the $Zr3d_{5/2}$ and $Zr3d_{3/2}$, indicating the synthesis of ZrO_2. The wide-angle XRD patterns were carried out to evaluate the crystal structure of ZrO_2. As shown in Fig S1c, the ZrO_2 synthesized by P123 only (marked ZrO_2-0) shows the diffraction peak at a 2θ angle of 30.2°, 34.9°, 50.2°, and 58.9°, indicating the formation of tetragonal phase ZrO_2 [30, 31]. As for ZrO_2-1 (synthesized by using AMTE only), the XRD pattern presents a lower-crystallized ZrO_2 with mixed tetragonal/monoclinic phases [32]. However, the dual templated ZrO_2 only exhibits stable tetragonal phase ZrO_2 (Fig. S1d), indicating the addition of AMTE does not change the crystal structure. The small-angle XRD pattern (Fig. S2) shows one single broad diffraction peak at 2θ angle of around 1°, which indicates that all the dual-templated samples display typical mesostructure [11]. Moreover, the sharp diffraction peak of the ZrO_2 material prepared with the ratio of 0.01 P123/0.02 AMTE /0.7 $Zr(SO_4)_2$ (ZrO_2-0.02) suggests a more organized mesoporous framework [33].

3.1.3 Porosity

SEM, TEM, N_2 sorption isotherm, and Mercury intrusion porosimetry were employed to compare the pores structure among all the samples and determine that the

dual-templated samples have both mesoporous and macroporous structures.

From the SEM images in Fig. 2a-e, the architecture of multidimensional pores obtained by combining P123 and AMTE as a dual template is evident. In addition, the hierarchical porous ZrO_2 obtained using 0.02 mol AMTE appears as well-organized macropores compared with the other ZrO_2 materials synthesized using different AMTE content. Moreover, Fig. S3 shows the SEM images of single templated ZrO_2 materials. It can be clearly observed that although ZrO_2-0 shows abundant porosity, the pore size is much smaller compared with dual-templated ZrO_2. However, ZrO_2-1 presents a larger pore structure with lower porosity. It can be concluded that both of the single-templated samples might show poor application for adsorption of macromolecule proteins due to smaller pore size or lower porosity, respectively. Actually, in the synthesis of multiscale porous ZrO_2, P123 serves as a template for the mesopores and as a stabilizer to maintain the ordered structure. AMTE is composed of phenolic hydroxyl and sulfonic groups, which can act as complexing agents to prevent the rapid hydrolysis rate of the metal source, and further facilitate the formation of well-organized porous structures. Moreover, the formation of a macroporous structure can be attributed to the amphiphilic nature and formation of micelles in solution. However, excess AMTE results in lower porosity as shown in Fig. 2e, which is attributed to the collapse of the pore structure during calcination of the organic template. From the SEM images of all the samples, the ZrO_2-0.02 shows a better pore structure and possesses both mesopores and macropores. TEM was employed to elucidate the hierarchical porosity of ZrO_2-0.02. The pore structure with different sizes can be observed clearly from the low electron density spots in Fig. 2f.

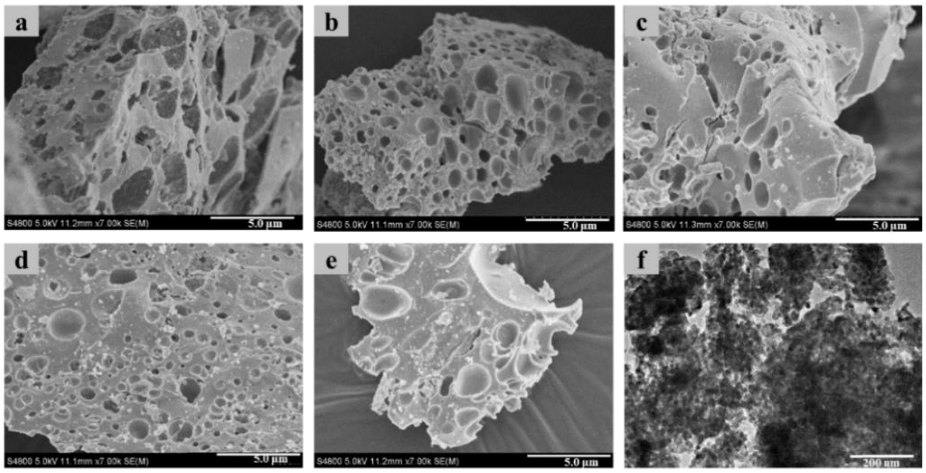

Fig. 2. SEM image of ZrO_2 synthesized using 0.01 mol P123, 0.7 mol $Zr(SO_4)_2$ and different content of AMTE (a~e: 0.01, 0.02, 0.03, 0.04, 0.05 mol AMTE, respectively, marked ZrO_2-0.01, ZrO_2-0.02, ZrO_2-0.03, ZrO_2-0.04, ZrO_2-0.05, respectively) (f) TEM images of ZrO_2-0.02

The porous properties can be further evaluated using the N_2 sorption isotherm. It can be seen that all the dual-templated ZrO_2 prepared by different content of AMTE display similar type IV isotherms with a remarkable H3 hysteresis loop at a relative pressure of 0.4~0.8 p/p_0 (Fig. 3a-e), suggesting the existence of mesoporous structure, which might be attributed to the effect of P123 [24]. The relative pressure of the hysteresis loop tends to increase with the increase of AMTE content, indicating the production of larger pores by increasing the amount of AMTE [34, 19]. Fig. 4. shows the pore size distribution of the sample. We can observe the increased amounts of AMTE from 0.01 mol to 0.02 mol lead to a more uniform pore size distribution. However, when the mounts of AMTE increased from 0.03 mol to 0.05 mol a decreased uniformity of pore size distribution was observed. The relative pore parameters of ZrO_2 in Table 1 show the surface area gradually decreases and the average pore size increases with the increase of AMTE. Combining the analysis of SEM, the sample synthesized by 0.02 mol AMTE facilitate more uniform pore size distribution with relatively larger surface area and pore diameter. Fig. 5 displays the N_2 sorption isotherm and pore size distribution of ZrO_2 materials synthesized by using P123 or AMTE only as a single template. Compared with dual-templated ZrO_2 material, it can be clearly observed ZrO_2-0 material presents the isotherm with H1 hysteresis loop at the relative pressure of 0.4, indicating the highly uniform pore size distribution. And the pore size distribution curve clearly shows that ZrO_2-0 has a higher surface area and smaller

average pore size (6.8 nm). The observation in Fig. 5b' and the comparison of pore structure parameters in Table 1 indicate that AMTE facilitates formation of larger pore sizes but with a lower specific surface area. Therefore, combining P123 and AMTE as a dual template can result in hierarchical porosity with a relatively higher surface area.

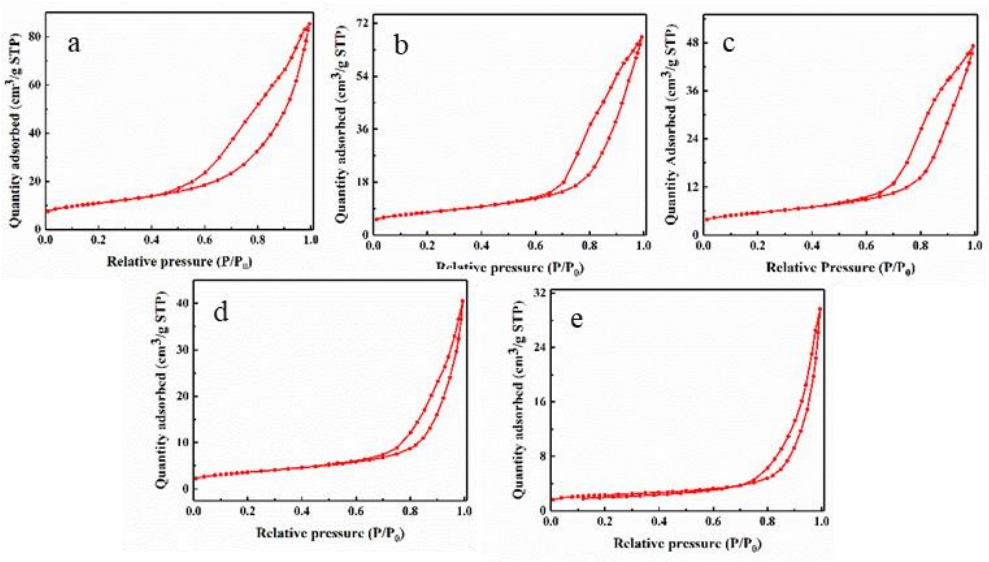

Fig. 3. N_2 adsorption-desorption isotherms of ZrO_2 (a~e: ZrO_2-0.01, ZrO_2-0.02, ZrO_2-0.03, ZrO_2-0.04, ZrO_2-0.05, respectively)

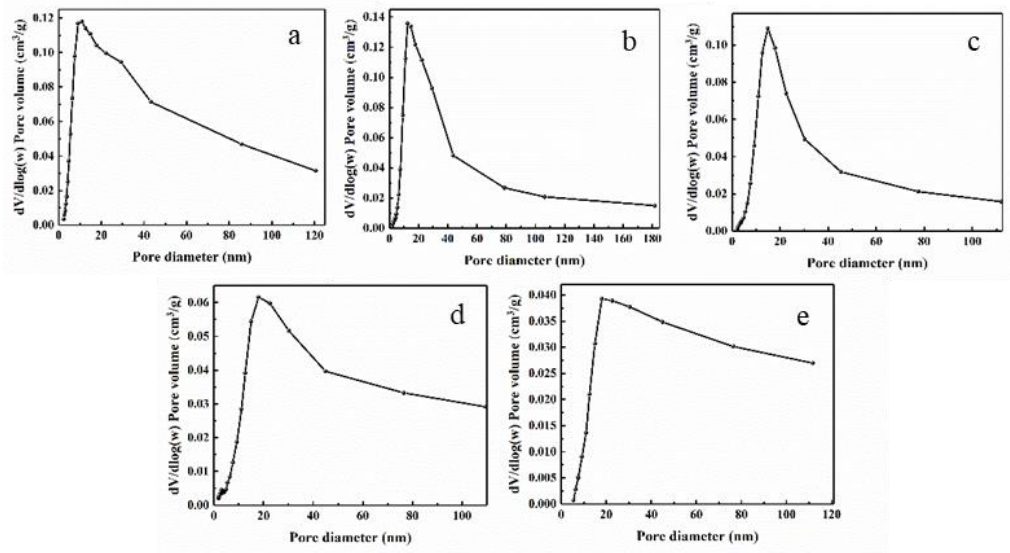

Fig. 4. the pore size distribution from BJH method of ZrO_2 (a~e: ZrO_2-0.01, ZrO_2-0.02, ZrO_2-0.03, ZrO_2-0.04, ZrO_2-0.05, respectively)

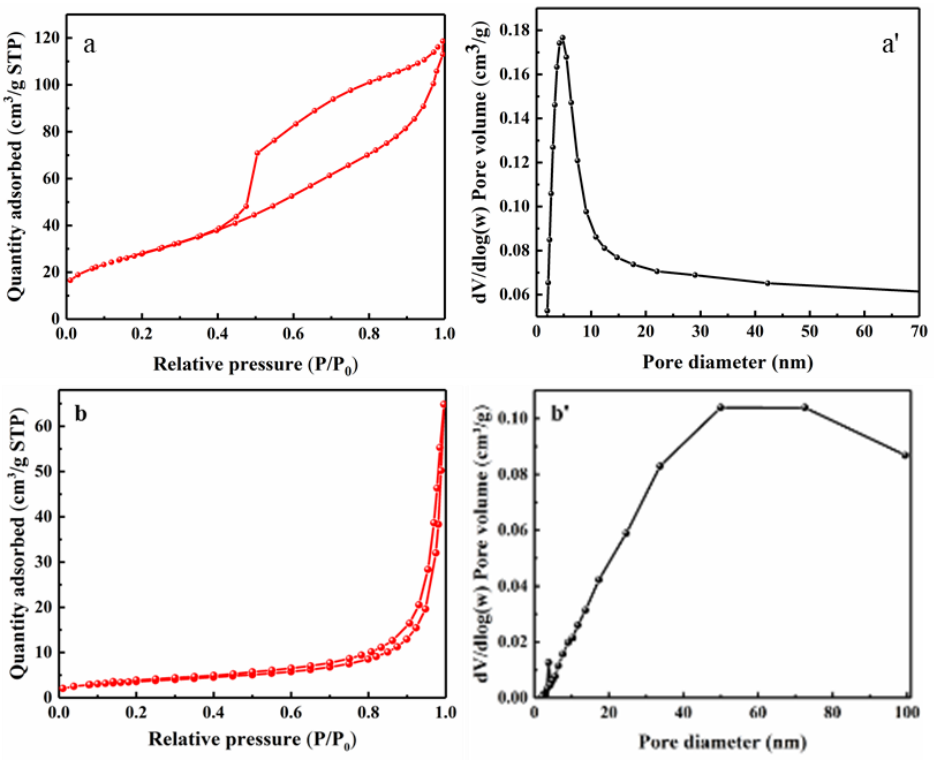

Fig. 5. N_2 adsorption-desorption isotherms of (a) ZrO_2-0 and (b) ZrO_2-1, respectively;(a') and (b') are the corresponding pore size distribution from BJH method of ZrO_2 materials

Table 1. The relative pores parameters of hierarchical porous ZrO_2.

Sample	S_{BET} (m^2/ g)	Average pore diameter (nm)	V_{tot} (cm^3 /g)
ZrO_2-0	98.3587	6.42	0.1637
ZrO_2-0.01	38.3492	13.63	0.1307
ZrO_2-0.02	26.9814	15.43	0.1041
ZrO_2-0.03	19.5172	14.88	0.0726
ZrO_2-0.04	12.9054	19.05	0.0614
ZrO_2-0.05	12.7972	27.36	0.0768
ZrO_2-1	7.8738	22.60	0.0445

In order to further prove the existence of macropores of ZrO_2-0.02, mercury intrusion porosimetry was employed to observe the distribution of pores size. As shown in Fig. 6, the average size of mesopores generated by using the P123 template is around 17 nm, which indicates a multiscale porous structure has been prepared successfully and is consistent with the results from the N_2 sorption isotherm. The macropores voids generated upon removal of the AMTE from the composite materials are 0.06~2.4 μm in diameter. However, the irregular macropore size distribution might be attributed to the existence of the branched structure of AMTE and the solvent [24].

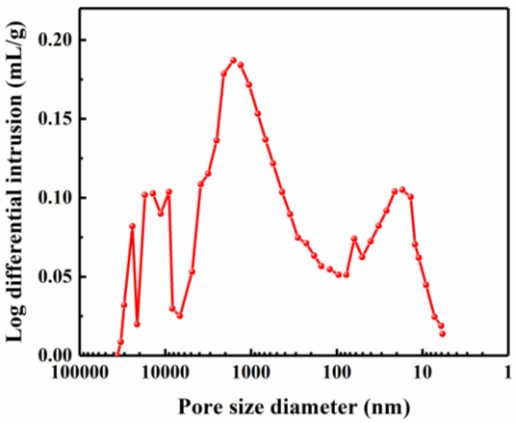

Fig. 6. The pore size distribution of ZrO_2-0.02 from mercury intrusion porosimetry

3.2 Application in protein adsorption

According to the above characterizations, ZrO_2-0.02 possesses hierarchical porosity compared with single-templated materials and shows better pore structure compared with other amounts of AMTE. Therefore, we choose it as an adsorbent to evaluate the application of hierarchical porous ZrO_2 materials in protein separation using BSA and Lyz (different molecular size) as protein models. Fig. S4 shows the variation of pH and protein adsorption capacity. It can be clearly observed that hierarchical porous ZrO_2 possesses maximum adsorption capacity for BSA at pH 5. As for the adsorption of Lyz, the adsorption capacity is decreased with increasing pH values. These tendencies are attributed to electrostatic interaction during the adsorption process [35].

3.2.1 Adsorption process and behavior

Fig. S5a shows the effect of time on Lyz adsorption on ZrO_2-0.02. As the results indicate, the adsorption process tends towards equilibrium after six hours. Adsorption kinetics curve of PFO and PSO models (Fig. 7) were employed to evaluate the adsorption rate and process of ZrO_2-0.02 with proteins. Table. 2 lists the relative kinetic parameters. It can be clearly observed that the PSO model can better describe the process of the experiments due to the larger correlation coefficients (R^2) and better experimental theoretical adsorption capacity (q_e), which indicates the chemical adsorption process [36]. Fig.S5b exhibits the protein concentration influence of Lyz adsorption with ZrO_2-0.02, which shows that the adsorption capacity of Lyz with ZrO_2-0.02 is increased from 17.1 mg/g to 45.5 mg/g by increasing the fresh concentration of Lyz. And the adsorption isotherms of Langmuir and Freundlich (Fig. 8) are used to

analyze the experiment data and protein adsorption behavior. The calculated data of the fitted curve are listed in Table 3, from which it can be concluded that the Langmuir model is more suitable to fit the experimental data owning to the higher R^2 value, indicating the homogeneous sorption process between adsorbent and adsorbate [37]. FT-IR spectra of Lyz before and after adsorption (Fig. S6) on ZrO_2-0.02 shows no obvious differences except for the intensity difference due to the presence of porous ZrO_2, suggesting the stability of the protein molecules during the sorption process.

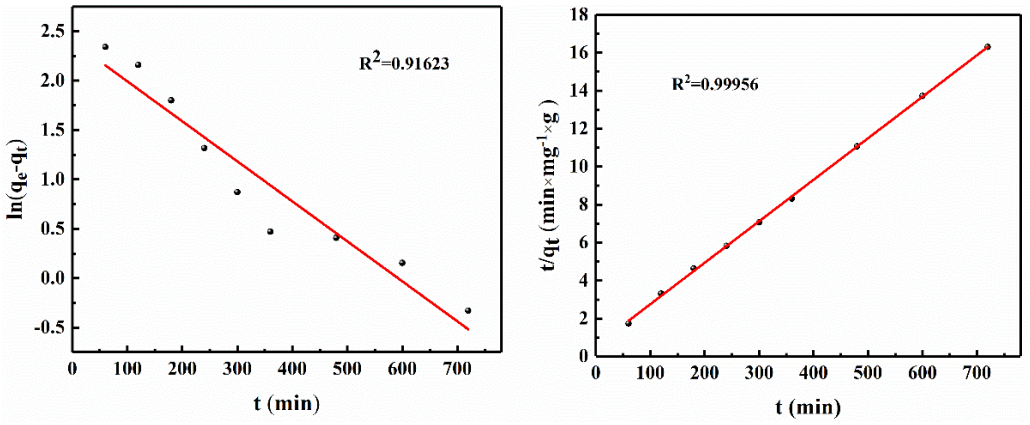

Fig. 7. Adsorption kinetic data of Lyz onto ZrO_2-0.02 fitted by two kinetic (PFO (left) and PSO (right)) equations.

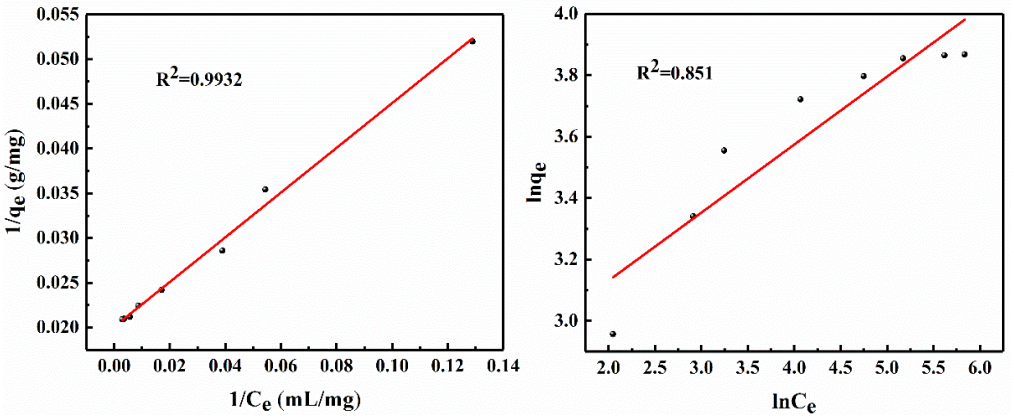

Fig. 8. Adsorption isotherms of Lyz adsorption on ZrO_2-0.02 fitted by the Langmuir (left) and Freundlich (right) models

Table 2. Relative calculated parameters of PFO and PSO kinetic models for Lyz adsorption onto ZrO_2-0.02

PFO			PSO		
k_1 (min^{-1})	q_e (mg/g)	R^2	k_2 (g/mg/min)	q_e (mg/g)	R^2
4.05×10^{-3}	11.007	0.91623	8.42×10^{-4}	45.746	0.99956

Table 3. Relative calculated parameters of Langmuir and Freundlich models for Lyz adsorption onto ZrO_2-0.02

Langmuir			Freundlich		
b (L/g)	Q_m (mg/g)	R^2	n	k	R^2
8.02×10^{-2}	49.826	0.9932	4.514	14.701	0.851

3.2.2 Adsorption advantage of hierarchical porous ZrO_2 on macromolecular proteins

Due to the different hydrodynamic size of BSA ($3.8\times3.8\times14$ nm^3) [38] and Lyz ($1.9\times2.5\times4.3$ nm^3) [39], a mixture of the two proteins acts as the model to confirm the hierarchical porosity is more suitable for the adsorption of macromolecular proteins. Quantitative measurements using UV-vis spectroscopy was employed to compare the adsorption capacity directly among dual-templated ZrO_2 (ZrO_2-0.02) and the ZrO_2 prepared using P123 or AMTE only (ZrO_2-0 and ZrO_2-1). The adsorption results are shown in Fig. 9. It can be clearly observed that all these three samples show almost similar adsorption capacity for Lyz (43 mg/g) but only ZrO_2-0.02 has better adsorption performance for BSA (35.4 mg/g). This is because the pore size of all three samples is large enough to transfer protein with smaller molecular size like Lyz. But only ZrO_2-0.02 possesses both macropores and mesopores, which is more conducive to the mass transfer of the larger molecular size of BSA. In addition, compared with some other adsorbents used in the literature [Table 4.], our hierarchical porous ZrO_2 materials have the potential for application in the field of protein adsorption especially for larger proteins.

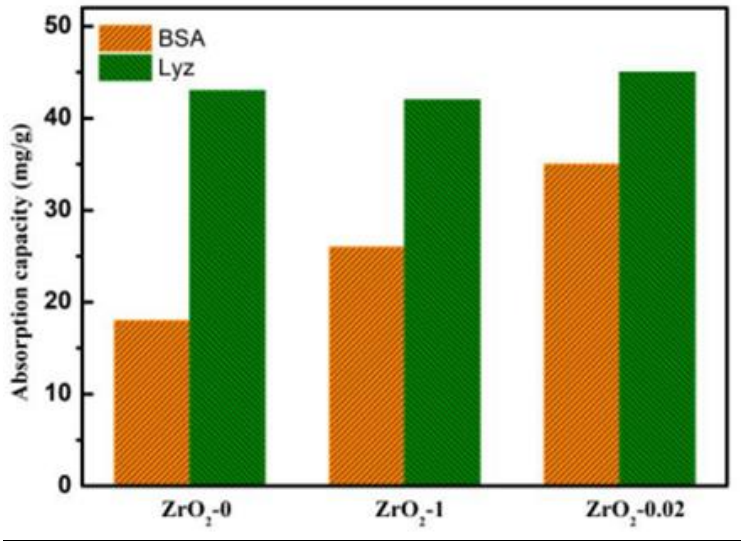

Fig. 9. Adsorption capacity of ZrO_2 prepared under different conditions towards Lyz and BSA

Table 4. Comparison of adsorption capacity of different adsorbents

Adsorbing material	Adsorbate	Contact time	Adsorption capacity	Refs
(SA-g-E)-g-APST/SO_3H	Lyz	180 min	37.68 mg/g	[40]
Agars-PEG-S	BSA	180 min	3.2 mg/g	[41]
Lyz-MIP cryogel	Lyz	60 min	22.9 mg/g	[42]
Lyz-imprinted QDs	Lyz	720 min	33.2 mg/g	[43]
AuNPs-LDH	Hb	500 min	42.5 mg/g	[44]
Macro-/mesoporous silica	BSA	360 min	16.6 mg/g	[37]
Hierarchical porous ZrO_2	Lyz/BSA	360 min	43/35.4 mg/g	Present study

3.2.3 Real sample test

To investigate the practical protein adsorption capacity of hierarchical porous ZrO_2, leather softening wastewater was used as a feed solution. As clearly shown in Fig. 10, ZrO_2-0.02 maintains considerable adsorption capacity for proteins in real-world samples due to the obvious reduction of absorbance, which is superior to the sample synthesized by using AMTE and P123 as a single template. These results are in accordance with the porosity analysis using the N_2 sorption isotherm. Therefore, hierarchical porous ZrO_2 combining the biomass materials of AMTE and P123 as a dual template exhibits excellent real-world sample adsorption capability.

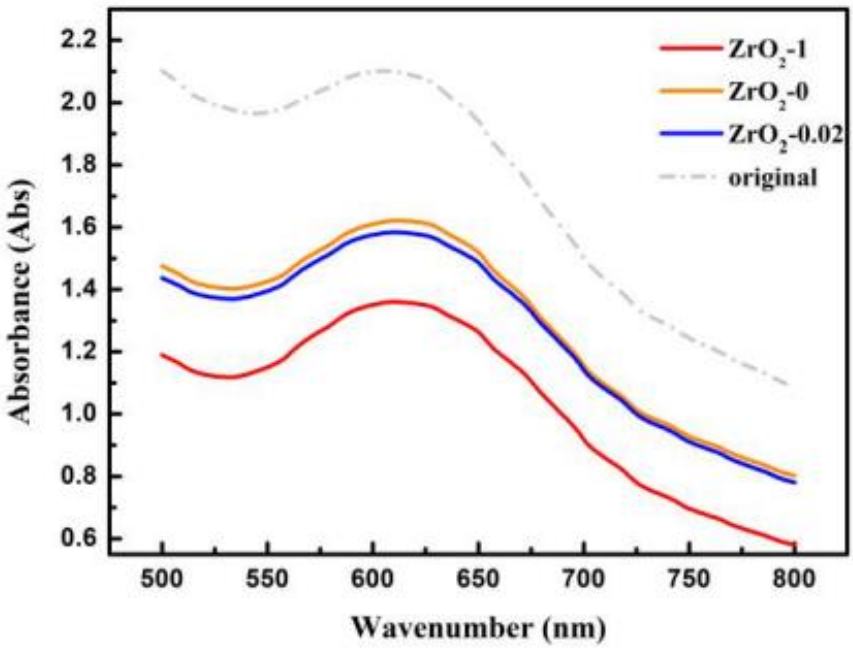

Fig. 10. UV spectrum of leather softening wastewater. The gray dashed line represents the original wastewater before adsorption. The red, orange and blue curves represent the wastewater adsorbed by ZrO_2-1, ZrO_2-0 and ZrO_2-0.02, respectively. The reduction of absorbance indicates that the proteins were adsorbed by the ZrO_2 materials.

4. Conclusions

In conclusion, we have developed a dual-templated hierarchical porous ZrO_2 material prepared using a simple and environmentally friendly synthetic route, which is reproducible and suitable for large-scale production. While for this research, we focused on the preparation of ZrO_2 materials. Our approach in combining biomass materials and traditional amphiphilic triblock copolymer as dual-templates is versatile, making it suitable for extension into the preparation of any porous oxide materials with hierarchical porosity. Compared with ZrO_2 synthesized using P123 and AMTE as a single template, the dual template method is critical for the formation of multi-size porous structures, making them excellent candidates for the protein adsorption with large molecules. In addition, compared with other adsorption materials, our synthesized hierarchical porous ZrO_2 material can be used as a candidate to adsorb large-sized proteins. The adsorption experiments with protein mixtures and leather softening wastewater demonstrate the practical potential of the hierarchical porous ZrO_2 materials for the adsorption and regeneration of protein from wastewater.

Supporting Information

Notes

The authors declare no competing financial interest.

Acknowledgements

Thanks for the Youth Innovation Team of Shaanxi Universities and Program of Introducing Talents of Shaanxi Province, which give us financial support to study this work. TDJ wishes to thank the Royal Society for a Wolfson Research Merit Award.

References

[1] Y. Wang, G. C. Wang, Y. Xiao, Y. L. Yang, R. K. Tang, Yolk-shell nanostructured Fe_3O_4@$NiSiO_3$ for selective affinity and magnetic separation of His-tagged proteins, ACS. Appl. Mater. Interfaces. 6 (2014) 19092-19099.

[2] J. Li, X. P. Liao, Q. X. Zhang, S. Bi, Adsorption and separation of proteins by collagen fiber adsorbent, J. Chromatogr. B. 928 (2013) 131-138.

[3] J. W. Zhao, F. Gao, Y.L. Fu, W. Jin, P.Y. Yang, D.Y. Zhao, Biomolecule separation using large pore mesoporous SBA-15 as asubstrate in high performance liquid chromatography, Chem. Commun. 7 (2002) 752-753

[4] Y. S. Tao, H. Kanoh, L. Abrams, K. Kaneko, Mesopore-modified zeolites: preparation, characterization, and applications, Chem. Rev. 106 (2006) 896-910

[5] M. Wu, Q. Meng, Y. Chen, L.X. Zhang, M. L. Li, X. J. Cai, Y. P. Li, P. C. Yu, L. L. Zhang, J. L. Shi, Nanoparticles: Large pore-sized hollow mesoporous organosilica for redox-responsive gene delivery and synergistic cancer chemotherapy, Adv. Mater. 28 (2016) 1963-1969.

[6] J. Wei, Y. Ren, W. Luo, Z. K. Sun, X.W. Cheng, Y.H. Li, Y.H. Deng, A. A.lzatahry, D.l-Dahyan, D.Y. Zhao, Ordered mesoporous alumina with ultra-large pores as an efficient absorbent for selective bioenrichment, Chem. Mater. 29 (2017) 2211-2217.

[7] G. A. Seisenbaeva, O. A. Dudarko, V. G. Kessler, Hierarchically porous zirconia through precursor-directed large-scale synthesis, J. Sol-Gel. Sci. Techn. 90 (2019) 140-148.

[8] D. K. A. Xu, J. J. Zhu, H. Q. Liu, B.S. Kang, Fabrication of ordered macroporous rutile titania at low temperature, New J. Chem. 26 (2002) 819-821.

[9] Y. Zheng, Y. G. Wei, K. Z. Li, X. Zhu, H. Wang, Y. H. Wang, Chemical-looping steam methane reforming over macroporous CeO_2-ZrO_2 solid solution: Effect of

calcination temperature, Int. J. Hydrogen Energ. 39 (2014) 13361-13368.

[10] G. L. Shi, F. Yu, Y. Wang, D. Pan, X. Yan, R. Li, Facile synthesis of micro-mesoporous alumina-zirconia nanocrystals with tailoring texture, Chem. Phys. Lett. 709 (2018) 41-45.

[11] H. Chen, J. Gu, J. Shi, Z. Liu, J. Gao, M. Ruan, D. Yan, A Composite Surfactant Route for the Synthesis of Thermally Stable and Hierarchically Porous Zirconia with a Nanocrystallized Framework, Adv. Mater. 17 (2005) 2010-2014.

[12] H. Wang, H. Chen, B. Ni, K. Wang, T. He, Y. L. Wu, X. Wang, Mesoporous ZrO_2 nanoframes for biomass upgrading, ACS. Appl. Mater. Interfaces. 9 (2017) 26897-26906.

[13] Y. S. Ko, Y. U. Kwon, Mesoporous zirconia thin films with three-dimensional pore structures and their application to electrochemical glucose detection, ACS. Appl. Mater. Interfaces. 5 (2013) 3599-3606.

[14] P. D. Yang, T. Deng, D. Y. Zhao, P. Y. Feng, D. Pine, B. F. Chmelka, G. M. Whitesides, G. D. Stucky, Hierarchically ordered oxides, Science. 282 (1999) 2244-2246.

[15] C. M. A. Parlett, K. Wilson, A. F. Lee, Hierarchical porous materials: catalytic applications, Chem. Soc. Rev. 42 (2013) 3876-3893.

[16] Z. L. Yan, L. J. Fu, H. M. Yang, J. Ouyang, Amino-functionalized hierarchical porous SiO_2-AlOOH composite nanosheets with enhanced adsorption performance, J. Hazard. Mater. 344 (2018) 1090-1100.

[17] K. Zhang., L. L. Xu, J. G. Jiang, N. Calin, K. F. Lam, S. J. Zhang, H. H. Wu, G. D. Wu, B. Albela, L. Bonneviot, P. Wu, Facile large-scale synthesis of monodisperse mesoporous silica nanospheres with tunable pore structure, J. Am. Chem. Soc. 135 (2013) 2427-2430.

[18] Z. F. Li, X. L. Wei, T. Ming, J. F. Wang, T. Ngai, Dual templating synthesis of hierarchical porous silica materials with three orders of length scale, Chem. Comm. 46 (2010) 8767-8769.

[19] Z. Gao, I. Zharov, Large pore mesoporous silica nanoparticles by templating with a nonsurfactant molecule, tannic acid, Chem. Mater. 26 (2014) 2030-2037.

[20] Y. Chen, S. K. Lunsford, Y. Song, H. X. Ju, P. Falaras, V. likodimos, A. G. Kontos, D. D. Dionysiou, Synthesis, characterization and electrochemical properties of mesoporous zirconia nanomaterials prepared by self-assembling sol-gel method

with Tween 20 as a template, Chem. Eng. J. 170 (2011) 518-524.

[21] P. With, A. Heinrich, M. Lutecki, S. Fichtner, B. Böhringer, R. Gläser, Zirconia with defined particle morphology and hierarchically structured pore system synthesized via combined exo- and endotemplating, Chem. Eng. Technol. 33 (2010) 1712-1716.

[22] D. Kwon, B. G. Cha, Y. Cho, J. Min, E. B. Park, S. J. Kang, J. Kim, Extra-large pore mesoporous silica nanoparticles for directing in vivo M_2 macrophage polarization by delivering IL-4, Nano. Lett. 17 (2017) 2747-2756.

[23] T. T. Qiang, C. Liang, Q. Zhang, X. H. Liu, A sustainable and cleaner speedy tanning system based on condensed tannins catalyzed by laccase, J. Clean. Prod. 197 (2018) 1117-1123.

[24] G. L. Drisko, A. Zelcer, V. Luca, R. A. Caruso, G. J. de A. A. Soler-Illia, One-pot synthesis of hierarchically structured ceramic monoliths with adjustable porosity, Chem. Mater. 22 (2010) 4379-4385.

[25] G. T. Li, T. T. Li, Y. L. Li, L. B. An, W. Li, Z. M. Zhang, Preparation of pH-controllable nanofibrous membrane functionalized with lysine for selective adsorption of protein, Colloid Surf. A 531 (2017) 173-181.

[26] M. Díaz, M. A. Villa-García, R. Duarte-Silva, M. Rendueles, Preparation of organo-modified kaolinite sorbents: The effect of surface functionalization on protein adsorption performance, Colloid Surf. A 530 (2017) 181-190.

[27] M. M. Bradford. A Rapid and Sensitive Method for the Quantitation of Microgram Quantities of Protein Utilizing the Principle of Protein-Dye Binding, Anal. Biochem. 72 (1976) 248-254.

[28] P. Wang, C. C. Jia, J. Li, P. Yang, Ti^{3+}-doped TiO_2 (B)/anatase spheres prepared using thioglycolic acid towards super photocatalysis performance, J. Alloy. Compd. 780 (2019) 660-670.

[29] D. H. Deng, H. Wua, X. P. Liao, B. Shi, Synthesis of unique mesoporous ZrO_2-carbon fiber from collagen fiber, Micropor. Mesopor. Mater. 116 (2008) 705-709.

[30] S. Rana, S. Mallick, K. M. Parida, Facile method for synthesis of polyamine-functionalized mesoporous zirconia and its catalytic evaluation toward henry reaction, Ind. Eng. Chem. Res. 50 (2011) 2055-2064.

[31] F. Ma, H. Zhao, Supercritical fluid extraction of a novel template from mesoporous

zirconia and the effect on porous structure, Chinese. J. Chem. Eng. 21 (2013) 698-700.

[32] H. L Liu, X. F Sun, C. Q. Yin, C. Hu, Removal of phosphate by mesoporous ZrO_2, J. Hazard. Mater. 151 (2008) 616-622.

[33] K. M. Parida, S. Mallick, P. C. Sahoo, S. K. Rana, A facile method for synthesis of amine-functionalized mesoporous zirconia and its catalytic evaluation in Knoevenagel condensation, Appl. Catal. A-General. 381 (2010) 226-232.

[34] H. Du, J. Bai, C. Zuo, Z. F. Xin, J. B. Hu, A hierarchical supra-nanostructure of HKUST-1 featuring enhanced H_2 adsorption enthalpy and higher mesoporosity, Cryst. Eng. Comm. 13 (2011) 3314-3316.

[35] W. J. Xu, Y. Z. Chen, W. S. Zhang, B.J. Li, Fabrication of graphene oxide/bentonite composites with excellent adsorption performances for toluidine blue removal from aqueous solution, Advanced Powder Technology 30 (2019) 493-501

[36] X. C. Xu, Y. Li, D. Y. Yang, X. D. Zheng, Y. Y. Wang, J. M. Pan, T. Zhang, J. C. Xu, F. X. Qiu, Y. S. Yan, C. X. Li, A facile strategy toward ion-imprinted hierarchical mesoporous material via dualtemplate method for simultaneous selective extraction of lithium and rubidium, J. Clean. Prod. 171 (2018) 267-274.

[37] M. Arshadi, H. Eskandarloo, M. K. Abdolmaleki, A. Abbaspourrad, A biocompatible nanodendrimer for efficient adsorption and reduction of Hg(II), ACS Sustainable Chem. Eng. 6 (2018) 13332-13348.

[38] Z. K. Sun, Y. H. Deng, J. Wei, D. Gu, B. Tu, D. Y. Zhao, Hierarchically ordered macro-/mesoporous silica monolith: tuning macropore entrance size for size-selective adsorption of proteins, Chem. Mate. 23 (2011) 2176-2184.

[39] L. Medda, A. Salis, M. Monduzzi, Lysozyme adsorption and release from ordered mesoporous materials, J. Phys. Chem. C. 114 (2010) 19928-19934.

[40] T. S. Anirudhan, T. A. Rauf, Lysozyme immobilization via adsorption process using sulphonic acid functionalized silane grafted copolymer, Colloid. Surface. B. 107 (2013) 1-10.

[41] F. P. Roudsari, M. R. Mehrnia, H. Kaghazian, Towards rational design of porous nanostructured biopolymeric microparticles for biomacromolecules separation: A case study of intraparticle diffusion facilitation and BSA adsorption on agarose microspheres, Mat. Sci. Eng. C-Mater. 93 (2018) 518-528.

[42] N. Bereli, M. Andac, G. Baydemir, R. Say, I. Y. Galaev, A. Denizli, Protein recognition via ion-coordinated molecularly imprinted supermacroporous cryogels,

J. Chromatogr. A. 1190 (2008) 18-26.

[43] W. Zhang, X. W. He, Y. Chen, W. Y. Li, Y. K. Zhang, Molecularly imprinted polymer anchored on the surface of denatured bovine serum albumin modified CdTe quantum dots as fluorescent artificial receptor for recognition of target protein, Biosens. Bioelectron. 31 (2012) 84-89.

[44] L. Jin, D. D. He, Z. X. Li, M. Wei, Protein adsorption on gold nanoparticles supported by a layered double hydroxide, Mater. Lett. 77 (2012) 67-70.